Saudi Pharmaceutical Journal 32 (2024) 102100

HOSTED BY

Contents lists available at ScienceDirect

Saudi Pharmaceutical Journal

journal homepage: www.sciencedirect.com

Original article

Preparing a novel baicalin-loaded microemulsion-based gel for transdermal delivery and testing its anti-gout effect

Yingzhou Wang [a,1], Mingxue Liu [a,1], Junjie Li [a,1], Peipei Jiang [a], Di Han [a], Hongling Zhang [b], Lingyun Xu [a,*], Yinsheng Qiu [c,**]

[a] School of Life Science and Technology, Wuhan Polytechnic University, Wuhan 430023, China
[b] College of Medicine and Health Science, Wuhan Polytechnic University, Wuhan 430023, China
[c] School of Animal Science and Nutrition Engineering, Wuhan Polytechnic University, Wuhan 430023, China

ARTICLE INFO

Keywords:
Baicalin
Microemulsion-based gel
Skin penetration and retention
Gouty arthritis
Analgesic and anti-inflammatory activity

ABSTRACT

We previously demonstrated that baicalin had efficacy against gouty arthritis (GA) by oral administration. In this paper, a novel baicalin-loaded microemulsion-based gel (B-MEG) was prepared and assessed for the transdermal delivery of baicalin against GA. The preparation method and transdermal capability of B-MEG was screened and optimized using the central composite design, Franz diffusion cell experiments, and the split-split plot design. Skin irritation tests were performed in guinea pigs. The anti-gout effects were evaluated using mice. The optimized B-MEG comprised of 50 % pH 7.4 phosphate buffered saline, 4.48 % ethyl oleate, 31.64 % tween 80, 13.88 % glycerin, 2 % borneol, 0.5 % clove oil and 0.5 % xanthan gum, with a baicalin content of (10.42 ± 0.08) mg/g and particle size of (15.71 ± 0.41) nm. After 12 h, the cumulative amount of baicalin permeated from B-MEG was (672.14 ± 44.11) $\mu g \cdot cm^{-2}$. No significant skin irritation was observed following B-MEG application. Compared to the model group, B-MEG groups significantly decreased the rate of auricular swelling ($P < 0.01$) and number of twists observed in mice ($P < 0.01$); and also reduced the rate of paw swelling ($P < 0.01$) and inflammatory cell infiltration in a mouse model of GA. In conclusion, B-MEG represents a promising transdermal carrier for baicalin delivery and can be used as a potential therapy for GA.

1. Introduction

As the most prevalent noninfectious arthritis in males aged 40 and above, gouty arthritis (GA) is caused by the deposition of crystallized monosodium urate (MSU) within joints or surrounding tissues, manifesting as localized redness, swelling, heat, and pain (Keller and Mandell, 2021). Eventually, GA culminates in bone destruction and joint deformities. Current pharmacotherapies primarily consist of oral formulations for nonsteroidal anti-inflammatory drugs (NSAIDs), colchicine, or corticosteroids, may encounter limitations such as malabsorption, adverse effects from first-pass metabolism, gastrointestinal irritation, hepatotoxicity, and fluctuating plasma levels, reducing efficacy (Ren et al., 2020; Wilson and Saseen, 2016). Transdermal drug delivery systems (TDDS) offer a promising alternative by circumventing the variability in absorption and metabolism associated with oral treatment (Hu et al., 2022). Transdermally-delivered drugs can directly access joint cavities, facilitating rapid onset while enhancing bioavailability for gout therapy. However, the stratum corneum poses a barrier for transdermal preparations, particularly for molecules larger than 500 Da or with moderate lipophilicity (Ali et al., 2022). To surmount this challenge, permeation enhancers (Hmingthansanga et al., 2022; Kováčik et al., 2020) and nanosystems such as microemulsions (Souto et al., 2022) have been employed in TDDS.

Microemulsions (ME) are homogeneous, stable solutions characterized by low viscosity and small particle size (10–100 nm) that can effectively increase drug solubility and absorption for transdermal delivery (Szumała and Macierzanka, 2022). Microemulsion-based gels (MEGs) are formulated by incorporating suitable gel matrices (Špaglová

* Corresponding author at: School of Life Science and Technology, Wuhan Polytechnic University, Xuefu South Road 68, Changqing Garden, Wuhan 430023, China.
** Corresponding author at: School of Animal Science and Nutrition Engineering, Wuhan Polytechnic University, Xuefu South Road 68, Changqing Garden, Wuhan 430023, China.
E-mail addresses: doctorxly9898@163.com (L. Xu), qiuyinsheng6405@163.com (Y. Qiu).
[1] Contributed equally to this work.

https://doi.org/10.1016/j.jsps.2024.102100
Received 9 March 2024; Accepted 12 May 2024
Available online 14 May 2024

et al., 2021). Serving as innovative transdermal carriers, MEGs combine the advantages of MEs and gels, encompassing high drug loading capacity, transdermal capability, good bioadhesion, and sustained release (Talaat et al., 2019). Extensive literature demonstrated the potential of MEGs in enhancing drug delivery via transdermal routes (Cao et al., 2017; Shinde et al., 2018).

Baicalin, a flavonoid extracted from *Scutellaria baicalensis Georgi,* exhibits diverse bioactivities including antibacterial, anti-inflammatory, anti-allergic, anticonvulsant, anticancer and anti-ultraviolet effects (Bao et al., 2022; Wen et al., 2023). Our prior investigations have shown that baicalin exhibited *in vitro* and *in vivo* efficacy against gouty arthritis (Wen et al., 2017, 2018), and also mitigates hyperuricemic nephropathy via inhibition of the PI3K/AKT/NF-κB signaling pathway (Liu et al., 2023; Xiang et al., 2021). However, baicalin encounters challenges such as poor aqueous solubility, low lipophilicity, and extensive first-pass metabolism with oral administration (Mi et al., 2021). With its relatively low molecular weight (446.4 Da) and anti-gout properties, baicalin emerges as a promising candidate for transdermal delivery via microemulsion-based gels to improve bioavailability.

In this study, a novel baicalin-loaded microemulsion-based gel (B-MEG) was methodically designed and optimized using the central composite design, Franz diffusion cell experiments, and the split-split plot design. A comprehensive series of experiment was carried out to assess B-MEG, encompassing evaluation of its physicochemical properties, *ex vivo* skin permeation kinetics, skin compatibility, and *in vivo* efficacy against inflammatory, painful and gouty arthritis.

2. Materials and methods

2.1. Materials

Baicalin (>90 % purity) was obtained from Sichuan Xieli Pharmaceutical Co., Ltd., China. Baicalin standards (93.3 % purity) were from National Institutes for Food and Drug Control, China. Diclofenac diethylamine emulgel (DDAE, 0.2 g diclofenac sodium/20 g) was from Beijing Novartis Pharmaceutical Co., Ltd., China. Isopropyl myristate, caprylic capric triglyceride, polyoxyethylene hydrogenated castor oil (RH40), ethyl oleate, polyethylene glycol 400 (PEG400), polyethylene glycol 200 (PEG200), carboxymethyl cellulose sodium, glycerol, oleic acid, 1,2-propylene glycol, Tween 80, absolute ethanol, polyoxyethylene castor oil (R40), poloxamer 188, poloxamer 407, xanthan gum, borneol, and clove oil were acquired from commercial sources at reagent grade purity. Uric acid (>99 % purity) was from Sigma Co., Ltd., USA. Xylene was from Tianjin Tianli Chemical Reagent Co., Ltd., China. Acetic acid was from Shandong West Asia Chemical Industry Co., Ltd., China. All other unspecified reagents were of analytical grade.

2.2. Animals

All animal experiments were carried out in accordance with the guidelines of the National Institutes of Health for the Care and Use of Laboratory Animals. Experimental protocols were approved by Animal Welfare Ethics Committee of Wuhan Polytechnic University (Approval number: WPU20180925008 and WHPU20191022026).

Male and female Kunming mice and guinea pigs were obtained from the Laboratory Animal Center of Huazhong University of Science and Technology (Wuhan, China). The animals were housed under standard conditions (22 ± 2 °C, 12 h light/dark cycle) and provided standard feed and water *ad libitum*.

2.3. Solubility of baicalin

To identify optimal components for microemulsion, the solubility of baicalin was measured in various oils, surfactants, and co-surfactants by shake flask method (Shinde et al., 2018). Excess baicalin was added to 5 mL of each vehicle (oil, surfactant, or co-surfactant), shaken at 150 rpm for 48 h in a reciprocating incubator shaker (Zhongbei, Changzhou, China) at 25 ± 2℃, and centrifuged at 6000 rpm for 30 min using a centrifuge (Xiangyi, Hunan, China). The supernatants were diluted with methanol and filtered through a 0.22 μm membrane, and assayed by high-performance liquid chromatography (HPLC) (Waters 2707, USA).

Baicalin was analyzed by HPLC using a Diamonsil C18 column (5 μm, 250 × 4.6 mm) with a mobile phase of methanol/water/phosphoric acid (55:45:0.04, v/v/v) at a flow rate of 1.0 mL/min. The detection wavelength was set at 277 nm (Lu et al., 2019). The assay exhibited linearity within the range of 5–160 μg/mL with percentage recoveries of 97 %-104 %. The baicalin retention time was 6.95 min.

2.4. Compatibility investigation

The compatibility of microemulsion phases is critical for stability. The investigation of phase compatibility proceeded as follows: (1) Surfactant and cosurfactant were mixed (Smix) at a ratio of 3:1 (w/w). (2) Smix was combined with oil and baicalin at 9:1:0.05 (w/w/w). (3) Water was combined with the above mixture at a ratio of 3:2 (w/w). (4) Mixtures were observed for clarity and absence of opacity after 1 month at room temperature. Baicalin was included in the initial screening to assess microemulsion stability, because drug incorporation might effect the alteration in phase behavior.

2.5. Construction of pseudo-ternary phase diagrams

Pseudo-ternary phase diagrams were constructed using the water titration method to determine concentration ranges of microemulsion components (Daryab et al., 2022; Ali et al., 2017). Oil and Smix (surfactant:cosurfactant) were mixed at ratios of 9:1, 8:2, 7:3, 6:4, 5:5, 4:6, 3:7, 2:8, and 1:9 (w/w). Water was added dropwise under stirring until clear microemulsions formed, as indicated by visual inspection. The water amounts were recorded and plotted to generate pseudo-ternary phase diagrams. Smix ratios of 1:1, 2:1, and 3:1 was evaluated. Microemulsion regions were calculated and compared.

2.6. Preparation, optimization and characterization of B-ME

2.6.1. Preparation of B-ME

Determined concentration of baicalin was combined with Tween 80, glycerin and ethyl oleate, and mixed well. Water was added to the mixture gradually and the solution was stirred continuously using a magnetic stirrer (Huyueming, Shanghai, China). After 1 h, the baicalin-loaded microemulsion (B-ME) was obtained.

2.6.2. Optimization of oil phase, surfactant and cosurfactant

Central composite design (CCD) is the most common method for response surface design (Cao et al., 2017), which enables efficient optimization with few experimental runs and high predictive accuracy (Lin et al., 2021). A 13-run, two-factor, five-level CCD was utilized to optimize this microemulsion formulation. Two factors, namely oil content (X_1) and Smix ratio (Km, X_2), were selected as independent variables based on phase diagrams. The baicalin saturation solubility (Y_1) and mean particle size (Y_2) were chosen as response variables. The model was fitting as the following polynomial regression equation (1) describing the influence of the independent variables on the response variables (Cao et al., 2017). Subsequently, contour and response surface plots of the independent and response variables were generated using Design-Expert 8.0 software.

$$Y = \beta_0 + \beta_1 X_1 + \beta_2 X_2 + \beta_3 X_1 X_2 + \beta_4 X_1^2 + \beta_5 X_2^2 \quad (1)$$

where Y is response variable; β_0 is intercept representing the arithmetic average of all quantitative outcomes of 13 runs; β_1-β_5 are coefficients computed from the observed experimental values of Y; X_1 and X_2 are coded levels of independent variables; X_1X_2 is factor interaction;

X_1^2 and X_2^2 is quadratic term.

2.6.3. Optimization of water content

To optimize water content, B-ME were prepared with 45 %, 50 %, 55 %, 60 % or 65 % water (w/w) while maintaining constant oil:surfactant: cosurfactant ratios. Baicalin content and skin permeation were assessed using Franz diffusion cells (Zhengtong, Tianjing, China) (Yang et al., 2017). The volume of the diffusion cell was 12 mL. Excised abdominal mouse skin was mounted between donor and receptor chambers (with a 1.77 cm^2 diffusion area). Take 1 g of each microemulsion with different water contents. The receptor contained pH 6.8 PBS at 32 ± 1 °C with stirring. B-ME (1 mL) were applied to the donor chamber. Receptor samples (1 mL) were taken at 1, 2, 4, 6, 8 h and replaced with blank PBS. Samples were filtered, and HPLC was used to detect baicalin content. The chromatographic conditions were as the same as mentioned in 2.3. The assay was linear over 4.25–136 μg/mL with percentage recoveries of 92.3 %-103 %. Cumulative permeability (Q) was calculated using the standard formula (2). Optimal water content was selected based on the maximal baicalin content and skin permeation.

$$Qn = \left[Cn^{*}V + \sum_{i=1}^{n-1} (C_i \times 1) \right] / A \quad (2)$$

In this formula (2), Qn is the cumulative permeability at the n sampling point in μg·cm^{-2}; Cn is the drug concentration measured at the n sampling point in μg/mL; V is the diffusion cell volume in mL; Ci is the drug concentration measured at the i (i ≤ n-1) sampling point in μg/mL; A is the effective transdermal area in cm^2.

2.6.4. Screening of water phase

Since baicalin stability depends on pH, four water phases were evaluated: purified water, and phosphate buffers at pH 6.5, 7.0, and 7.4. Microemulsions were prepared with excess baicalin using the optimized oil:surfactant:cosurfactant ratios identified previously. After centrifugation at 6000 rpm for 30 min, the pH was measured, and baicalin content was determined by HPLC method as mentioned in 2.6.3. An optimal water phase was selected to maximize drug loading and microemulsion stability. Buffered water phases were assessed to identify conditions maximizing baicalin stability and solubility.

2.6.5. Physicochemical properties and characterization of B-ME

The pH value of B-ME was measured using a pH meter (Starter2100, Ohaus, China). The size, polydispersity index (PDI) and zeta potential of B-ME were determined using a laser particle size analyzer (ZEN3600, Malvern, UK). The viscosity of B-ME was determined using a hybrid rheometer (HR-1, TA, USA).

The morphology of B-ME was observed using atomic force microscopy (AFM, Multimode 8-HR, Bruker, Germany). B-ME samples were diluted, deposited onto mica discs (10 μL), and dried at room temperature for 48 h (Wan et al., 2017). The samples were imaged and processed using Nanoscope software 1.5 (Nanoscope Systems, Korea).

The microstructure of B-ME was observed using transmission electron microscopy (TEM, H-7000FA, HITACHI, Japan). Diluted B-ME samples were applied to copper grids, dried for 5 min, and negatively stained with 1 % phosphotungstic acid (Daryab et al., 2022). The grids were imaged at appropriate magnification.

The stability of B-ME was assessed for storage at room temperature for over 3 months. Three batches were evaluated monthly for signs of creaming or phase separation by visual inspection. Samples were centrifuged at 8000 rpm for 15 min and analyzed for particle size and baicalin content by HPLC at 0, 1, and 3 months.

2.6.6. Drug loading and encapsulation efficiency of B-ME

According to the above optimized prescription, 5 batches of microemulsion containing 1.0 % baicalin were prepared. Take 0.1 g of microemulsion in a volumetric flask, and add methanol under ultrasound for 20 min to break the emulsion (Mishra et al., 2016). The content of baicalin was detected by HPLC as the same as mentioned in 2.3. The drug loading (DL) and encapsulation rate (ER) were calculated with formulas (3) and (4).

$$DL(\%) = [Wa/W'] \times 100 \quad (3)$$

$$ER(\%) = [Wa/W] \times 100 \quad (4)$$

In these formulas, *Wa* is the amount of drug in the microemulsion, *W* is the amount of drug added to the microemulsion, *W'* is the total mass of the microemulsion.

2.7. Preparation and Characterization of B-MEG

2.7.1. Preparation of B-MEG

To develop an optimal B-MEG for transdermal delivery, suitable gelling agents and permeation enhancers were screened. B-ME exhibited low viscosity and poor skin adhesion. Conversion to B-MEG by incorporating a gel matrix could prolong drug residence time in skin. Based on compatibility and safety observed in preliminary experiments, xanthan gum, sodium carboxymethyl cellulose, poloxamers 407 and 188, borneol, and clove oil were selected as potential B-MEG components to enhance viscosity and promote skin permeation.

A split-plot design was used to systematically screen potential B-MEG components, including gelling agents and permeation enhancers (Keinath, 2019). The gel matrix factors included 1.5 % sodium carboxymethyl cellulose, 0.5 % xanthan gum, and 10 % poloxamer (7 % poloxamer 407, 3 % poloxamer 188). Borneol (1 %, 2 %) and clove oil (0.5 %, 1 %) were evaluated as permeation enhancers. B-MEGs containing 1 % baicalin were tested in Franz diffusion cells using excised mouse skin. Receptor samples were taken at 4, 8, 12 h, analyzed by HPLC, and cumulative baicalin permeation was calculated. Cumulative permeability (Q) was calculated with formula (2). This approach allowed efficient screening of multiple formulation factors and levels to identify an optimal B-MEG composition.

2.7.2. Characterization of B-MEG

The morphology of B-MEG was also observed by AFM and TEM according to the methods described in 2.6.5.

B-MEG was assessed for phase separation by centrifugation at 8000 rpm for 15 min. The pH was measured using a pH meter. Particle size was determined by laser diffraction (ZEN 3600, Malvern, UK). Viscosity was measured using a hybrid rheometer at a temperature of 15 °C and a shear rate of 6.65 s^{-1} (HR-1, TA, USA).

B-MEG was subjected to heating–cooling cycle testing. Three batches were stored at 4 °C for 48 h followed by 40 °C for 48 h for a total of 3 cycles. Samples were then centrifuged at 3000 rpm for 10 min and visually inspected for evidence of precipitation or phase separation.

2.8. Drug-Excipient chemical interaction by FTIR

To further characterize possible interactions between the drug and excipient in the solid state, Fourier transform infrared spectroscopy (FTIR) was used. Baicalin (BA), blank microemulsion gel (MEG) and B-MEG were combined with potassium bromide at a ratio of 1:100 and homogeneously ground, and the tablets were formed and then scanned from 4000-500 cm^{-1} using an infrared spectrophotometer (FTIR-850, Gangdong Technology, China).

2.9. In vitro evaluation

2.9.1. Ex vivo permeation studies of B-MEG

The transdermal permeation of B-MEG (with enhancers), B-MEG (without enhancers), and B-ME (without enhancers) was compared using Franz diffusion cells at 32 ± 1 °C. Samples (0.3 g) containing 3 mg

baicalin were applied to donor chambers. Receptor samples (1 mL) were taken at 1, 2, 4, 6, 8, and 12 h and replaced with fresh buffer. Samples were analyzed by HPLC after filtration.

2.9.2. Skin retention test

After permeation testing, skin samples were washed, cut into pieces, and soaked in 2 mL of methanol overnight. The tissue was swirled for 10 min, centrifuged, and the supernatant was filtered. Baicalin content in the extracts was analyzed by HPLC to determine skin retention.

2.10. In vivo evaluation

2.10.1. Guinea pig skin irritation test

Skin irritation testing of B-MEG was performed in guinea pigs (Lan et al., 2021). Sixteen animals were divided into groups receiving single or multiple doses on intact or damaged skin (n = 4 per group, equal males: females). Abdominal hair was removed and 0.5 mL B-MEG (1 % baicalin) or blank MEG (control) was applied topically once or daily for 7 days. Skin reactions were observed and evaluated compared to the control. This standard approach determined potential irritation from single or repeated B-MEG exposure.

After B-MEG application, the site was occluded for 4 h then washed. Erythema, edema, and other skin reactions were evaluated at 1, 24, 48, and 72 h using a standard 0–4 scoring system (0 = none, 4 = severe) (Li et al., 2020a; Wang et al., 2017). The mean irritation score for each group was calculated according to formula (5), and irritation strength was graded according to Table 1. This approach allowed comprehensive evaluation of potential B-MEG skin irritation.

$$M = \sum (A + B)/n \tag{5}$$

In this formula, M is the mean irritation score for each group, A is total erythema score, B is total edema score, n is number of animals subjected.

2.10.2. Xylene-induced auricular swelling in mice

Many studies have shown that baicalin through oral route has obvious anti-inflammatory effects (Li et al., 2020b). Xylene induced ear edema is a well-accepted and popular model for evaluating anti-inflammatory activity. Male Kunming mice (n = 40, 25–30 g) were randomly divided into 4 groups, each of 10 mice: xylene model group, DDAE group, low-dose B-MEG (0.25 % baicalin) group, and high-dose B-MEG (1 % baicalin) group. The dosage of the DDAE group was 0.03 g per mouse, and the dosage of B-MEG (0.25 %) and B-MEG (1.0 %) were 0.1 g per mouse (Yin et al.,2011, Liang et al., 2019).

Drugs were applied to the left ear of each mouse and the model group was not treated. Two hours after drug administration, 0.05 mL of xylene was applied to the anterior and posterior surface of the left ear of each mouse, with the right ear serving as a control. 30 min after xylene administration, the mice were euthanized by cervical dislocation under anesthesia and both ears were severed. Circular sections were taken using a puncher with a diameter of 6 mm and weighed (Talaat et al., 2019). Swelling was assessed based on the difference between the weight of the left ear and the right ear. The swelling rate of each group was determined with the following formula (6) and compared with that of the model group.

$$R(\%) = [(W_l - W_R)/W_R] \times 100 \tag{6}$$

In this formula, R is swelling rate, W_R is right ear weight, W_l is left ear weight.

2.10.3. Acetic acid induced writhing in mice

In order to assess the analgesic activity of B-MEG, acetic acid induced writhing model was used. Male and female Kunming mice (n = 40, 18–22 g) were randomly divided into 4 groups, each of 10 mice (equal males: females): acetic acid model group, DDAE group, low-dose B-MEG (0.25 % baicalin) group and high-dose B-MEG (1 % baicalin) group. The dosage of the DDAE group was 0.05 g per mouse, and the dosage of B-MEG (0.25 %) and B-MEG (1.0 %) were 0.2 g per mouse.

The drug was evenly applied to the mice abdominal skin, while the model group received no treatment. Two hours after drug administration, 0.7 % acetic acid (0.2 mL/10 g BW (body weight)) was administered intraperitoneally, and the mice were immediately placed in transparent cages with no covers to observe the number of twists within 20 min. The contraction of abdominal musculature and the extension of hind limbs were used as observation indicators (Ghias et al., 2022).

2.10.4. Effect of B-MEG against acute gouty arthritis in mice

Monosodium urate (MSU) crystals were prepared as previously described (Cao, 2021) and characterized to confirm size ≥ 25 μm by laser diffraction and lack of endotoxin contamination.

Male Kunming mice (n = 40, 18–22 g) were randomly divided into 4 groups, each of 10 mice: gout model group, DDAE group, low-dose B-MEG (0.25 % baicalin) group, and high-dose B-MEG (1 % baicalin) group. The DDAE group received a dosage of 0.03 g/20 g BW, while both the B-MEG (0.25 %) and B-MEG (1.0 %) were administered a dosage of 0.2 g/20 g BW. Treatments were topically applied once daily for 7 days to the right toe. On day 7, acute gout was induced 1 h after the final treatment by injecting 0.04 mL of 0.2 % MSU crystals into the right hind paw (Fattori et al., 2020).

At the end of treatment, blood was collected from the orbital venous plexus. Serum was obtained by centrifugation of the collected blood and stored at −20 °C. Then mice were euthanized under anesthesia and paw samples were collected for histological analysis. The following outcome measures were assessed: (1) Paw swelling at 1, 2, 4, 6, 10, 24 h; (2) Inflammation scores (0–6 scale); (3) Paw histopathology (H&E staining). Calculated the swelling rate of mice paw according to the following formula (7) (Tian et al., 2021).

$$Swellingrate(\%) = [(V_a - V_b)/V_b] \times 100 \tag{7}$$

Where V_a is the volume of paw at different time intervals after inflammation, and V_b is the volume of paw before inflammation.

Table 1
Skin irritation scoring and skin irritation strength grading.

Skin irritation scoring	Score
Erythema	A
No erythema	0
Slight erythema	1
Noticeable erythema	2
Moderate-severe erythema	3
Severe erythema to slight eschar formation	4
Edema	B
No edema	0
Slight edema	1
Mild edema (The skin was raised and contoured)	2
Moderate edema (The skin was raised by about 1 mm)	3
Severe edema (The skin was raised by more than 1 mm and the range is enlarged)	4
Total scores (M)	Skin irritation strength grading
0–0.5	Non-irritating
0.5–2.0	Mildly irritating
2.0–6.0	Moderately irritating
6.0–8.0	Intensively irritating

2.11. Statistical analysis

The results were expressed as the mean ± standard deviation and analyzed by using IBM SPSS Statistics 24.0 software (IBM Inc., USA). One-way analysis of variance (ANOVA) was conducted to analyze all obtained results. *P*-values less than 0.05 were considered to be

significant, while *P*-values less than 0.01 were considered highly significant.

3. Results

3.1. Solubility of baicalin in different phases

The solubility of baicalin in various oils, surfactants and co-surfactants were shown in Table 2. Baicalin exhibited maximal solubility in the surfactant Tween 80, thus it was chosen for further investigation. Oleic acid reacted with baicalin, so isopropyl myristate, caprylic capric triglyceride, and ethyl oleate were chosen as oils. While ethyl acetate exhibited similar solubility to ethyl oleate, the latter was preferred due to its safety and compatibility. Glycerin, PEG 200, and PEG 400 were selected as co-surfactants due to their superior baicalin solubility compared to 1,2-propylene glycol and ethanol.

3.2. Compatibility among phases

The results of the compatibility among phases were shown in Table 3. There were three formulations which could form transparent and stable microemulsion, including isopropyl myristate/Tween 80/PEG 400, caprylic capric triglyceride/tween 80/glycerol and ethyl oleate/tween 80/glycerol.

3.3. Pseudo-ternary phase diagrams

As shown in Fig. 1, pseudo-ternary phase diagrams were constructed for microemulsions containing isopropyl myristate, caprylic capric triglyceride, or ethyl oleate as the oil phase. Across all tested surfactant: cosurfactant (Km) ratios, the ethyl oleate system displayed the largest microemulsion region, indicating optimal stability. During microemulsion preparation, an increase in the Km ratio often led to the appearance of a gel zone, complicating mixing processes. Hence, to mitigate this issue, the maximum Km value was capped at 2.5. For further optimization, an oil phase of 3–10 % and Km of 1–2.5 were selected to ensure stability while preventing liquid crystal formation. Based on the phase diagrams, ethyl oleate was identified as the optimal oil phase, and specific component ranges were defined to achieve a stable B-ME.

3.4. Optimization and characterization of B-ME

3.4.1. Optimization of oil phase, surfactant and cosurfactant

In CCD, the total sum of oil phase, Smix and water was fixed to 100 %. Based on the pseudo-phase diagram, the percentage of oil phase (X_1) was set to 3–10 %, the Km value (X_2) was set to 1–2.5, and the water phase ratio remained fixed at 55 %. The factors and corresponding levels were outlined in Table 4. The saturation solubility of baicalin (Y_1) and the average particle size (Y_2) of ME were selected as the evaluation indexes. DesignExpert 8.0 software was used to design and analyze 13 batches of four factorial points, four axial points, and five replicated center points prepared by the formulation in Table 4. The best fit model was represented as follows (8) and (9).

$$Y_1 = 2.41 - 0.05X_1 + 2.29X_2 - 0.02X_1X_2 - 7.66e^{-3}X_1^2 - 0.43X_2^2 \quad (8)$$

$$Y_2 = -152.47 + 35.98X_1 + 95.94X_2 - 2.47X_1X_2 - 2.05X_1^2 - 26.97X_2^2 \quad (9)$$

The *P* values of both models were less than 0.05, the lack of fit was all not significant, and they represented good model fitting (Cao et al., 2017). The response surface plots (3D) of drug loading and particle size are shown in Fig. 2A and 2B. The series variance analysis, including the model *F*-value, and the comparative values of R^2, are provided in Table 5.

The CCD successfully identified optimal levels of oil content (X_1) and Km (X_2) to maximize baicalin loading (Y_1) and minimize particle size (Y_2). The optimized B-ME contained X_1 4.03 % and X_2 2.28, predicting Y_1 4.84 mg/g and Y_2 15.01 nm. Experimental values for the optimized B-ME were Y_1 4.82 ± 0.15 mg/g and Y_2 14.49 ± 1.53 nm, aligning closely with the predicted values. The model effectively optimized a B-ME formulation with high drug loading and small particle size.

3.4.2. Optimization of water content

Franz diffusion cell method was used to optimize the ratio of water phase by comparing the transdermal characteristics of microemulsion prescriptions with different water contents. When the water content of B-ME was 45 %, baicalin content was the highest at 5.79 ± 0.01 mg/g (n = 3). As the water content of B-ME increased from 45 % to 65 %, baicalin content gradually decreased, reaching its lowest level of 3.72 ± 0.02 mg/g baicalin at 65 % water content. The transdermal amount of B-ME with different water contents were shown in the Fig. 2C. Increasing water content of B-ME from 45 % to 65 % improved permeation up to 50 % water. At > 50 % water, permeation decreased. Considering both drug loading and permeation, 50 % water content was optimal for B-ME. Water content affected baicalin solubility and release, with 50 % providing the best balance of loading and skin permeation. Therefore, the optimal microemulsion formulation was 4.48 % oil phase, 31.64 % Tween 80, 13.88 % glycerol and 50 % water. It was an oil-in-water

Table 2
Solubility of baicalin in various excipients (mean ± SD, n = 3).

Excipients	Name	Solubility (mg/mL)
Oils	Isopropyl myristate	0.038 ± 0.007
	Caprylic capric triglyceride	0.040 ± 0.005
	Ethyl oleate	0.009 ± 0.001
	Ethyl acetate	0.008 ± 0.001
	Oleic acid	Baicalin discolored
Surfactants	Tween 80	13.13 ± 0.26
	Cremophor R40	6.36 ± 0.13
	Cremophor RH40	7.68 ± 0.19
Cosurfactants	1,2-propylene glycol	0.53 ± 0.05
	Glycerin	1.91 ± 0.03
	Polyethylene glycol 400	8.05 ± 0.21
	Polyethylene glycol 200	2.49 ± 0.16
	Absolute ethanol	0.32 ± 0.05

Table 3
Compatibility among phases in microemulsion.

Prescriptions	Oil	Surfactant	Co-surfactant	Compatibility of microemulsion
1	Isopropyl myrisate	Tween 80	Glycerol	–
2	Isopropyl myrisate	Tween 80	Polyethylene glycol 200	–
3	Isopropyl myrisate	Tween 80	Polyethylene glycol 400	+
4	Caprylic capric triglyceride	Tween 80	Glycerol	+
5	Caprylic capric triglyceride	Tween 80	Polyethylene glycol 200	–
6	Caprylic capric triglyceride	Tween 80	Polyethylene glycol 400	–
7	Ethyl oleate	Tween 80	Glycerol	+
8	Ethyl oleate	Tween 80	Polyethylene glycol 200	–
9	Ethyl oleate	Tween 80	Polyethylene glycol 400	–

Note: "+" meant a stable and transparent microemulsion; "–" meant not.

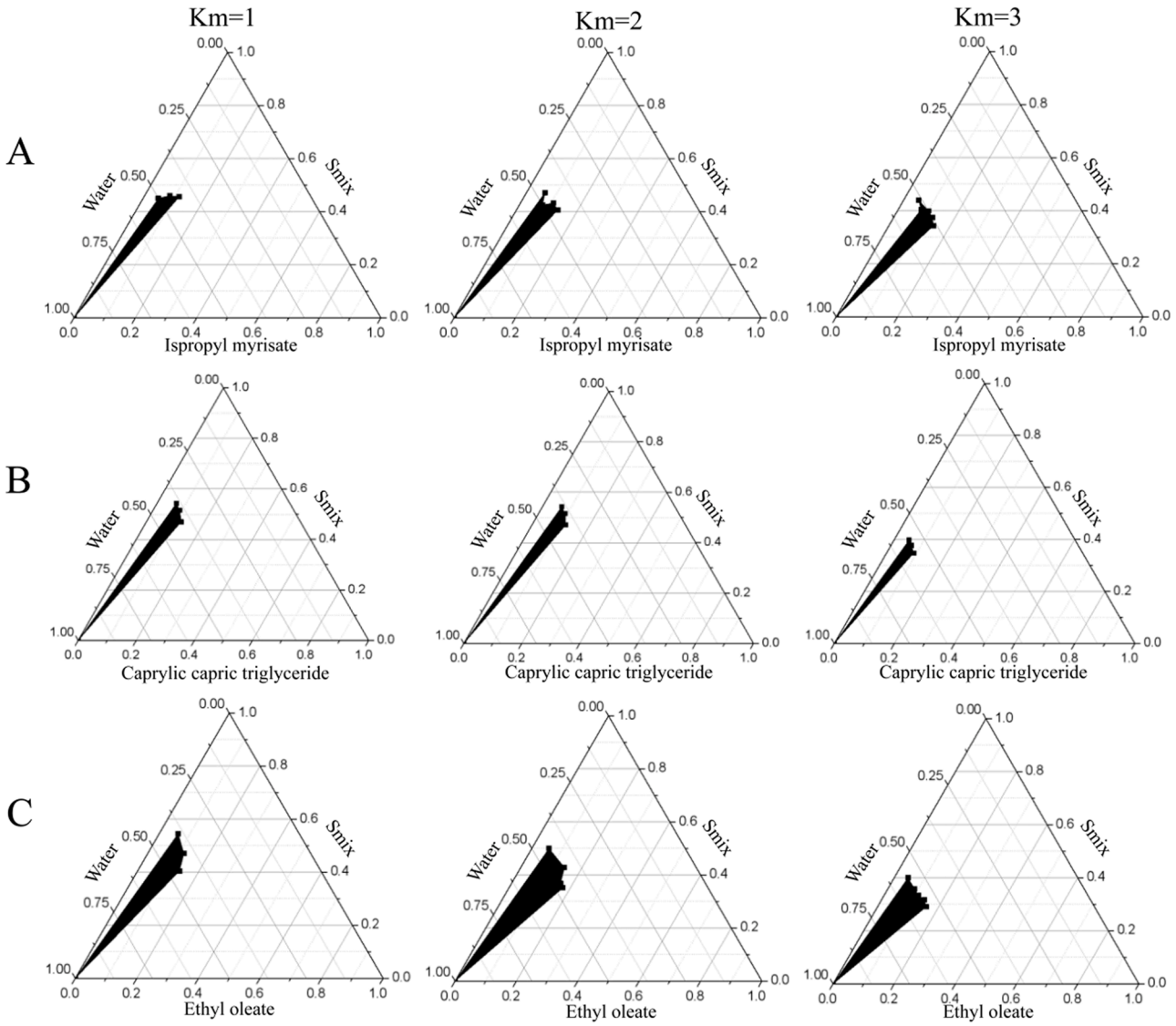

Fig. 1. Pseudo-ternary phase diagram with Tween 80 as surfactant, polyethylene glycol 400 as co-surfactant. Note: (A) Isopropyl myristate as oil phase and Km = 1, 2, 3, respectively. (B) Caprylic capric triglyceride as oil phase and Km = 1, 2, 3, respectively. (C) Ethyl oleate as oil phase and Km = 1, 2, 3, respectively.

microemulsion.

3.4.3. Screening of water phase

Comparison of drug loading and pH was conducted among four different aqueous microemulsions. When phosphate buffer (pH 7.4) was used as aqueous phase in B-ME formulation instead of purified water, baicalin loading increased significantly from 5.41 ± 0.03 to 10.56 ± 0.18 mg/g (n = 3), while the pH rose from 4.71 ± 0.02 (n = 3) to a skin-compatible 5.67 ± 0.02 (n = 3). The solubility of baicalin in the B-ME formulation (5.41 ± 0.03 mg/mL) was increased nearly 100-fold compared to that reported in the literature for baicalin dissolved in pure water (55.16 ± 0.53 μg/mL) (Ou et al., 2009). Phosphate buffer pH 7.4 optimized B-ME drug loading and pH for skin delivery. This prescription effectively increases the drug loading of B-ME (1 %) by optimizing the microemulsion composition ratio and selecting the water phase, which is 10 times that of the baicalin microemulsion prepared by Yang et al (0.1 %) (Yang et al., 2007).

3.4.4. Physical and chemical properties of B-ME

B-ME was an orange-yellow, clear and transparent liquid. Tyndall effect was one of the unique phenomena of microemulsion. As shown in Fig. 3A, B-ME had obvious Tyndall effect. The viscosity of B-ME was 0.078 Pa·s at 15 °C, 6.65 s^{-1}, as shown in Fig. 3B. The particles of B-ME were round, uniform in size and good in dispersion under transmission electron microscopy (TEM) (Fig. 3C) and atomic force microscopy (AFM) (Fig. 3D). The pH value of B-ME was 5.67 ± 0.02 (n = 3).

B-ME exhibited an average droplet size of 15.95 ± 0.77 nm (n = 3), polydispersity index of 0.131 ± 0.058 (n = 3), and zeta potential of –32.4 mv. B-ME was physically stable with no phase separation upon centrifugation. Particle size was 15.95 ± 0.77, 16.3 ± 0.20, and 17.02 ± 0.47 nm at 0, 1st, and 3rd month, respectively, n = 3. Drug loading also remained stable across 3 months in storage, which was 10.49 ± 0.33, 10.21 ± 0.51, and 10.62 ± 0.26 mg/g at 0, 1st, and 3rd month, respectively, n = 3.

3.4.5. Drug loading and encapsulation efficiency of B-ME

The average encapsulation efficiency of microemulsion was (95.28 ± 3.17)% (n = 3), and the average drug loading was (1.03 ± 0.04)% (n = 3).

Table 4
Independent variables and response variable in CCD for the microemulsion.

Number	Coded values of independent variables		Actual values of independent variables		Values of response variable	
	X_1	X_2	X_1 (%)	X_2	Y_1 (mg/g)	Y_2 (nm)
B-ME1	1.414	0	10	1.75	3.355	43.09
B-ME2	−1	−1	4.03	1.22	4.131	21.36
B-ME3	0	0	6.5	1.75	4.129	55.43
B-ME4	0	0	6.5	1.75	4.247	49.8
B-ME5	0	0	6.5	1.75	4.222	55.2
B-ME6	0	1.414	6.5	2.5	4.412	24.73
B-ME7	0	0	6.5	1.75	4.136	50.31
B-ME8	0	0	6.5	1.75	4.157	49.75
B-ME9	0	−1.414	6.5	1	3.408	49.55
B-ME10	1	1	8.97	2.28	3.877	35.68
B-ME11	−1	1	4.03	2.28	4.800	14.56
B-ME12	−1.414	0	3	1.75	4.783	11.41
B-ME13	1	−1	8.97	1.22	3.333	55.46
Independent variables		Levels				
		−α	−1	0	1	α
X_1 (%)		3	4.03	6.5	8.97	10
X_2		1	1.22	1.75	2.28	2.5

Note: The oil content (X_1) and Km ratio (X_2) were taken as the investigation factors. The solubility (Y_1) and microemulsion particle size (Y_2) were taken as evaluation indicators.

3.5. Preparation and Characterization of B-MEG

3.5.1. Screening of transdermal enhancer and gel matrix

In this study, tri-split-plot design was used to investigate several factors including the variety of the gel matrix, while simplifying the experimental steps and timings (Goulão et al., 2018; Wei et al., 2021). The results of the split-plot design experiment are shown in Table 6. Analysis of the split-plot design revealed significant differences between the various matrices and transdermal enhancers. The results of ANOVA are shown in Table 7. Significant synergistic effects occurred between borneol, gel matrix, and clove oil. Xanthan gum gel with 2 % borneol, 0.5 % clove oil, and 0.5 % xanthan gum exhibited the best performance based on permeation and stability. Although 1 % borneol showed high permeation, 2 % was selected for greater solubilization and stability.

3.5.2. Physical and chemical properties of B-MEG

As shown in Fig. 4A, B-MEG was orange-yellow and transparent gelatinous solution, and the handstand did not flow out, and had obvious Tyndall effect with a laser pointer. After centrifugation for 15 min at 8000 rpm, no stratification was observed. B-MEG showed the double characteristics of microemulsion and gel. The viscosity of B-MEG was 2.29 Pa·s at 15 °C, 6.65 s^{-1} (Fig. 4B), which increased markedly versus B-ME. B-MEG exhibited uniform particle distribution by TEM (Fig. 4C), pH 5.95 ± 0.10, size 15.71 ± 0.41 nm (Fig. 4D). As shown in Fig. 4E, microscopy revealed microemulsion droplets dispersed throughout the gel matrix by AFM. No change in appearance occurred after heating–cooling cycles. Characterization confirmed optimal properties of B-MEG as a transdermal delivery system.

In the heating–cooling cycle testing, B-MEG exhibited no phase separation. The findings of the comprehensive stability analysis have been published by us (Wang et al., 2022). As depicted in Supplementary Fig. 1, the pH, drug content, and particle size of B-MEG remained stable under conditions of high and low temperatures as well as high humidity. However, its stability was notably compromised under illumination, and

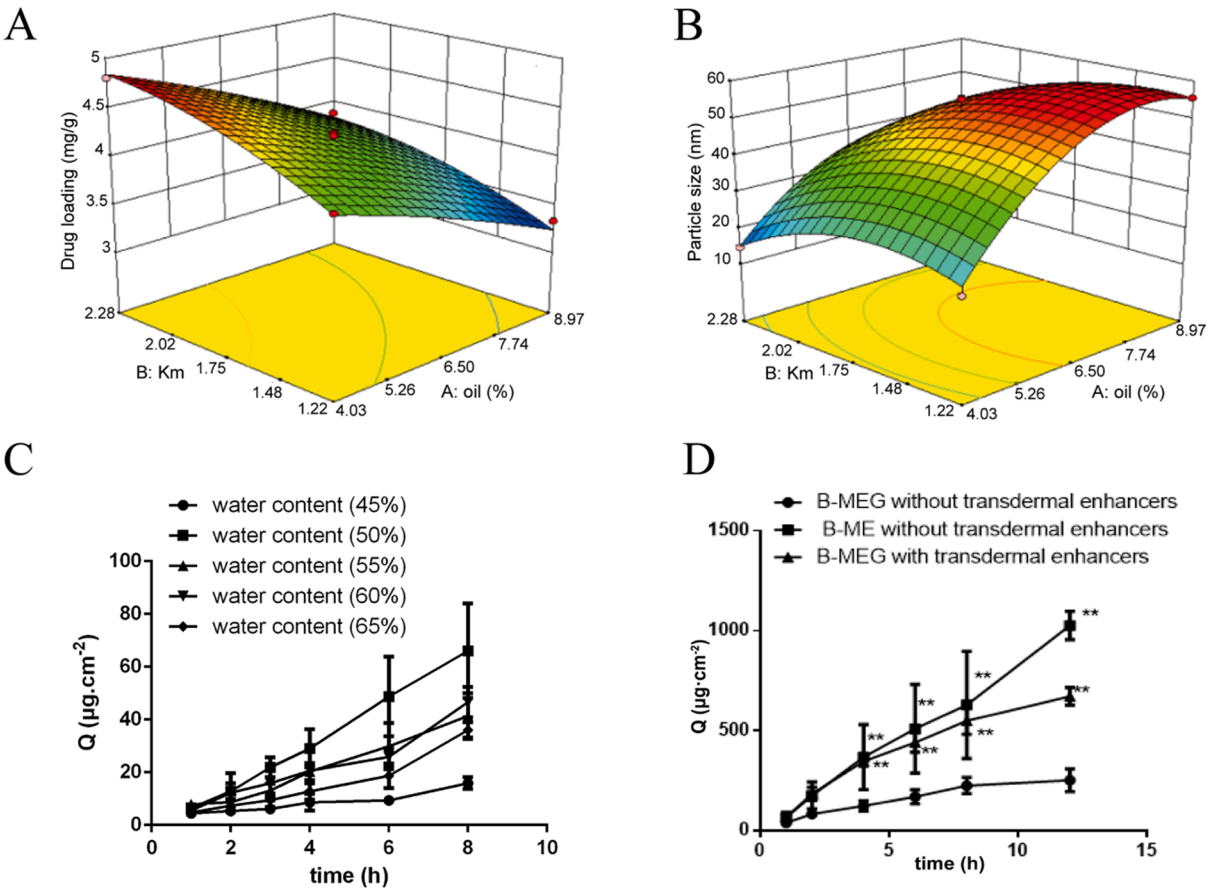

Fig. 2. Response surface plots (3D) of drug loading (A) and particle size (B); permeation profiles of B-ME (C) and B-MEG (D) during *ex vivo* permeation study (mean ± SD, n = 3). Note: Q is accumulative amount. Compared with B-ME without transdermal enhancers, $^{**}P < 0.01$.

Table 5
ANOVA results of central composite design.

Model	*F*	*P*	R^2	*Pred* R^2	*Adj* R^2	*AP*	*SD*	*C.V.%*
Y_1	109.73	<0.0001	0.9874	0.9329	0.9784	33.243	0.071	1.74
Y_2	81.44	<0.0001	0.9818	0.9312	0.9688	23.622	2.87	7.23

Note: Y_1 is solubility; Y_2 is microemulsion particle size. *F* represents the degree to which the factor influences the model. *P* represents the significance of the factor to the model. R^2 is relevant index which reflect a fitting degree. *Pred* R^2 (predicted R^2) and *adj* R^2 (adjusted R^2) are reasonably agree with each other represent a good model fitting. *AP* is "adeq precision", which measures the signal to noise ratio. SD, standard deviation. *C.V.%*, coefficient of variation.

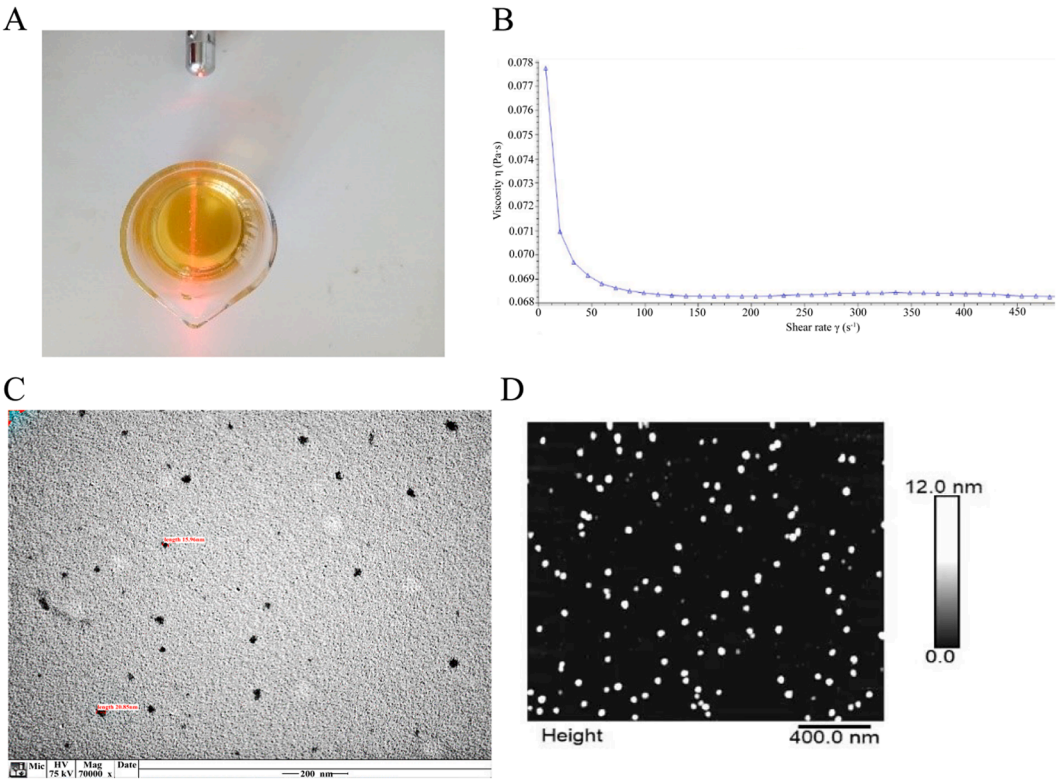

Fig. 3. Characterization of B-ME Note: (A) Tyndall effect. (B) Viscosity diagram. (C) Transmission electron microscopy figure (70,000×). (D) Atomic force microscope figure.

Table 6
Cumulative permeability of baicalin in split-plot design experiment (12 h).

Group	Q (μg·cm^{-2})					
	A_1		A_2		A_3	
	B (1 %)	B (2 %)	B (1 %)	B (2 %)	B (1 %)	B (2 %)
C (1 %)	0.85	0.9	0.84	1.08	0.66	0.9
C (0.5 %)	1.23	1.19	1.29	1.43	0.95	0.92
C (1 %)	0.82	0.94	0.8	1.21	0.87	0.98
C (0.5 %)	0.91	1.26	1.09	1.38	0.83	0.87

Note: A_1 is 0.5 % xanthan gum. A_2 is 1.5 % sodium carboxymethylcellulose. A_3 is 10 % poloxamer. B is borneol. C is clove oil. Q is cumulative permeability.

the viscosity significantly increased under high temperature. Consequently, it is advisable to store the preparation at low temperatures and shield it from light exposure.

3.6. Drug-Excipient chemical interaction

As shown in Fig. 5, in the infrared spectrum of baicalin, a prominent absorption peak ranging from 3250 cm^{-1} to 3500 cm^{-1}, attributed to the hydroxyl groups (Li et al., 2011). Additionally, the carbonyl peak appeared at 1680 cm^{-1}, the characteristic peak of the benzene ring at

Table 7
ANOVA results of split-splot design.

Source of variation		Degree of freedom	SS	Mean square	F	P
Primary area	District Group	1	0.003	0.003	0.731	>0.05
	A	2	0.286	0.143	32.063	<0.05
	ea	2	0.009	0.004	0.675	
Vice area	B	1	0.154	0.154	23.214	<0.01
	A × B	2	0.037	0.019	2.811	>0.05
	eb	6	0.040	0.007	0.591	
Sub region	C	1	0.260	0.260	23.251	<0.01
	A × C	2	0.087	0.044	3.885	>0.05
	B × C	1	0.007	0.007	0.625	>0.05
	A × B × C	2	0.160	0.080	7.143	<0.05
	ec	6	0.067	0.011		
	eabc	23	0.967			

Note: A is gel matrix. B is borneol. C is clove oil. ea is variation of A. eb is variation of B. ec is variation of C. eabc is total variation. *F* is homogeneity test of variance. *SS* is sum of squares of mean deviation. *P* represents a significant difference.

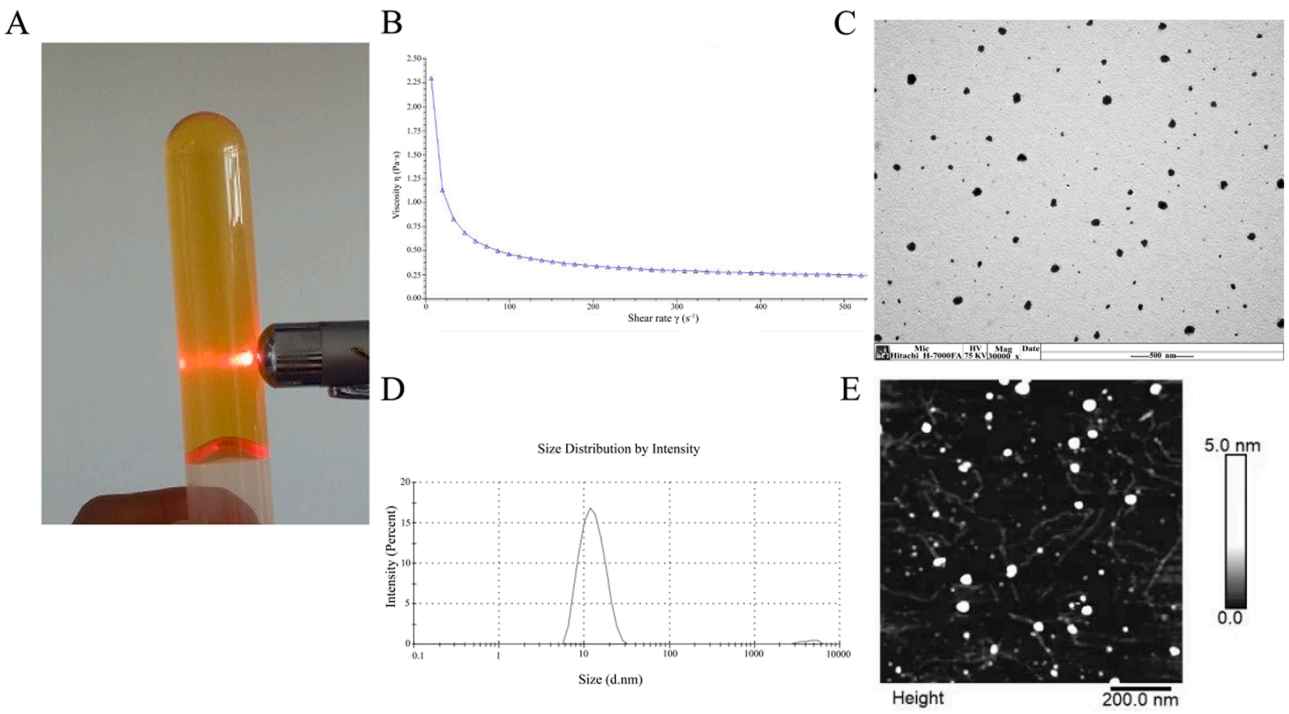

Fig. 4. Characterization of B-MEG Note: (A) Tyndall effect. (B) Viscosity diagram. (C) Transmission electron microscopy figure (30,000×). (D) Particle size. (E) Atomic force microscope figure.

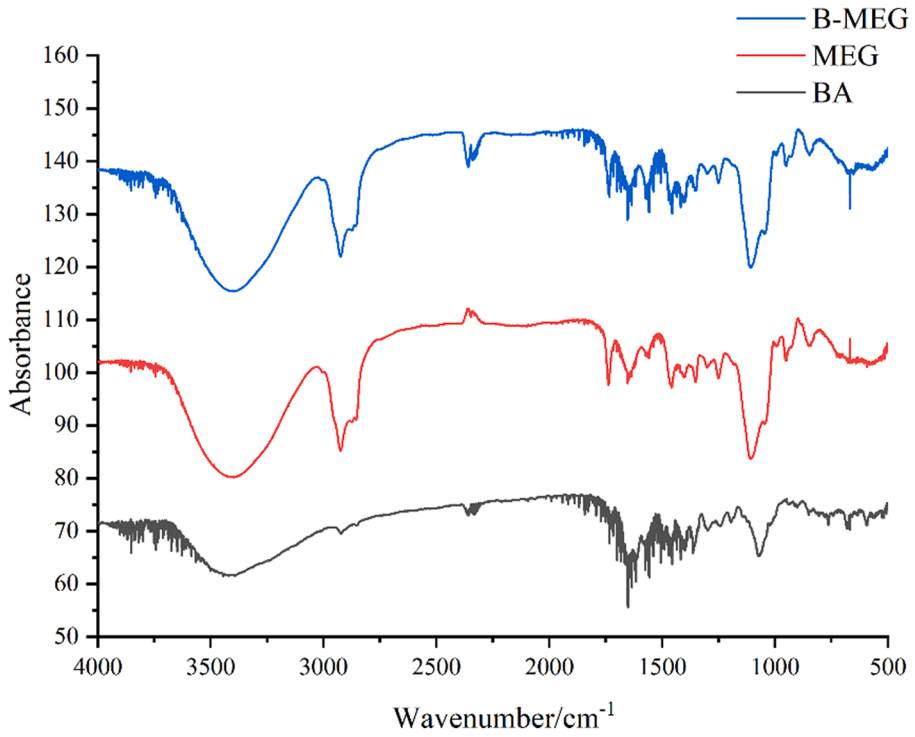

Fig. 5. Infrared spectra of baicalin (BA), blank microemulsion gel (MEG) and baicalin microemulsion gel (B-MEG).

1630 cm^{-1}, and the carbon–carbon double bond characteristic peak at 1450 cm^{-1}. The infrared spectrum of the blank microemulsion-based gel displayed a characteristic peak of saturated hydrocarbon at 2900 cm^{-1}. Notably, the infrared spectrum analysis revealed no emergence of new functional groups in B-MEG, suggesting that baicalin does not undergo reactions with excipients, and the excipients do not alter the structure of baicalin.

3.7. In vitro evaluation

3.7.1. Ex vivo permeability studies of B-MEG

Considering the antibacterial and anti-inflammatory effects of borneol and clove oil, both were chosen as penetration enhancer in this study. The aim was to achieve a synergistic effect with baicalin in anti-gout pharmacological activity while promoting penetration in

subsequent studies. As shown in the Fig. 2D, B-ME exhibited good permeation (1025.16 ± 70.47 μg·cm^{-2}) due to low viscosity enabling drug release. B-MEG without enhancers showed poor permeation (252.26 ± 56.73 μg·cm^{-2}) due to the viscous gel retarding release. Permeation enhancers significantly improved B-MEG permeation (672.14 ± 44.11 μg·cm^{-2}). These findings underscored the effectiveness of the permeation enhancers at facilitating baicalin release from B-MEG.

3.7.2. Skin retention test

The results of skin retention revealed that the gelling agent indeed increase the retention of the drug in the skin. Compared to the drug retention of B-ME after 12 h (10.1 ± 3.7 μg·cm^{-2}), both B-MEG formulations, with transdermal enhancers (27.3 ± 8.5 μg·cm^{-2}) and without transdermal enhancers (29.2 ± 5.8 μg·cm^{-2}), exhibited significant increase in skin retention.

3.8. In vivo evaluation

3.8.1. Skin irritation test results

As shown in Fig. 6, B-MEG showed no evidence of erythema, edema, pigmentation, bleeding, or thinning in guinea pig skin after single or multiple applications to intact or damaged skin. The irritation score was 0 at all the time points with no significant difference when compared to control gel or between groups. Guinea pigs remained active and healthy throughout. The results demonstrated that B-MEG did not induce skin irritation or dryness, supporting its safety for clinical use.

3.8.2. Anti-inflammatory and analgesic effects of B-MEG

As shown in Fig. 7A, compared to the model group, DDAE, 0.25 % B-MEG and 1.0 % B-MEG all significantly reduced the rate of auricular swelling in mice ($P < 0.01$). As shown in Fig. 7B, compared to the model group, DDAE, 0.25 % B-MEG and 1.0 % B-MEG significantly inhibited the writhing number of mice induced by acetic acid ($P < 0.05$ or $P < 0.01$). B-MEG showed good anti-inflammatory and analgesic effects.

3.8.3. B-MEG ameliorates acute gouty arthritis in mice

As shown in Fig. 7C and 7D, in the gout model, paw inflammation peaked at 6 h then decreased but remained edematous at 24 h, maybe aligning with the timing of MSU-induced IL-1β production (Wen et al., 2018). Compared to the model group, both 0.25 % and 1.0 % B-MEG significantly reduced paw inflammation score at 24 h ($P < 0.01$), and also significantly inhibited MSU-induced edema from 2 h to 24 h in a dose-dependent manner ($P < 0.05$ or $P < 0.01$). These results demonstrated that topical B-MEG effectively suppressed acute inflammation in

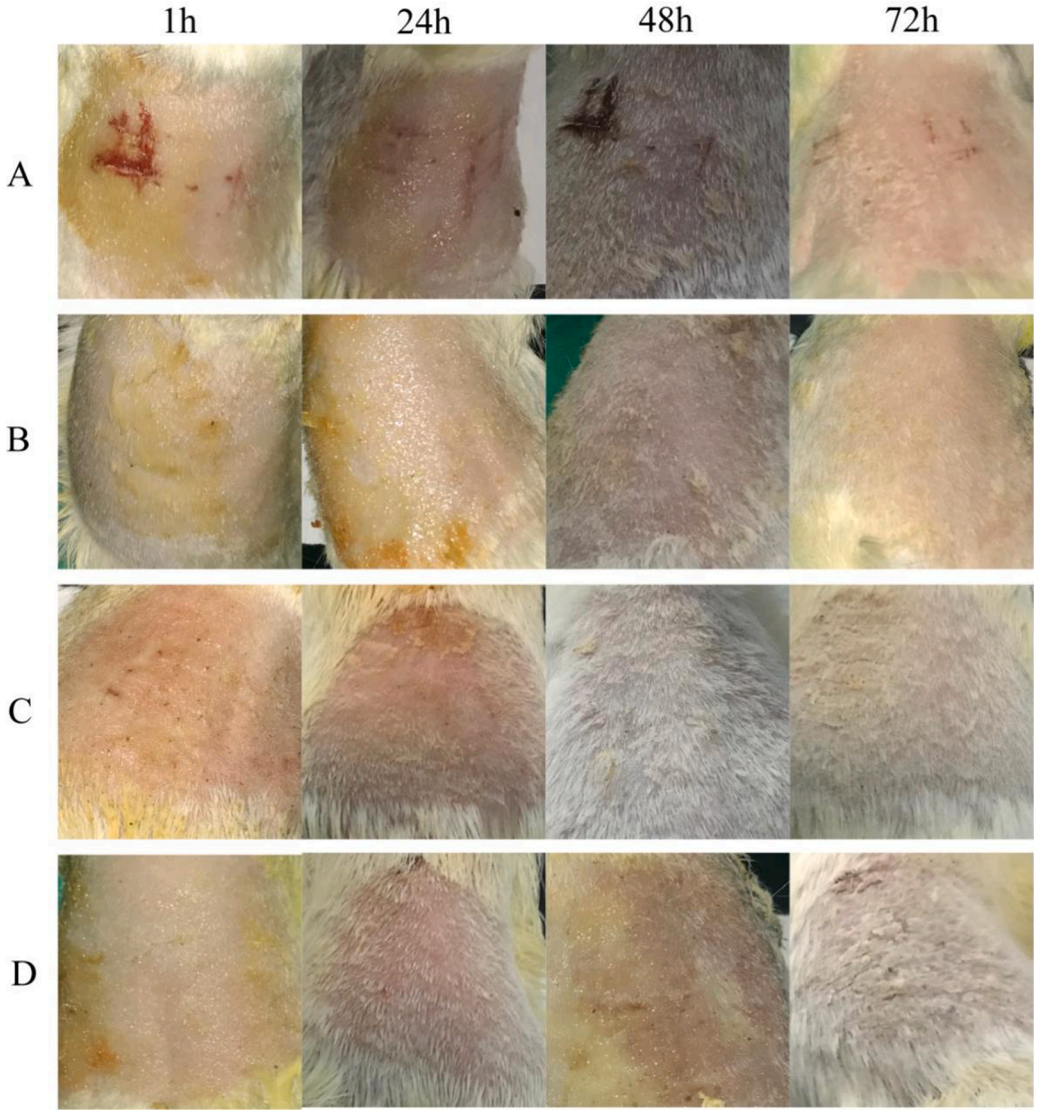

Fig. 6. Pictures of skin irritation from single and multiple administration in guinea pigs Note: (A) Single administration on damaged skin. (B) Single administration on complete skin. (C) Multiple administration on damaged skin. (D) Multiple administration on complete skin.

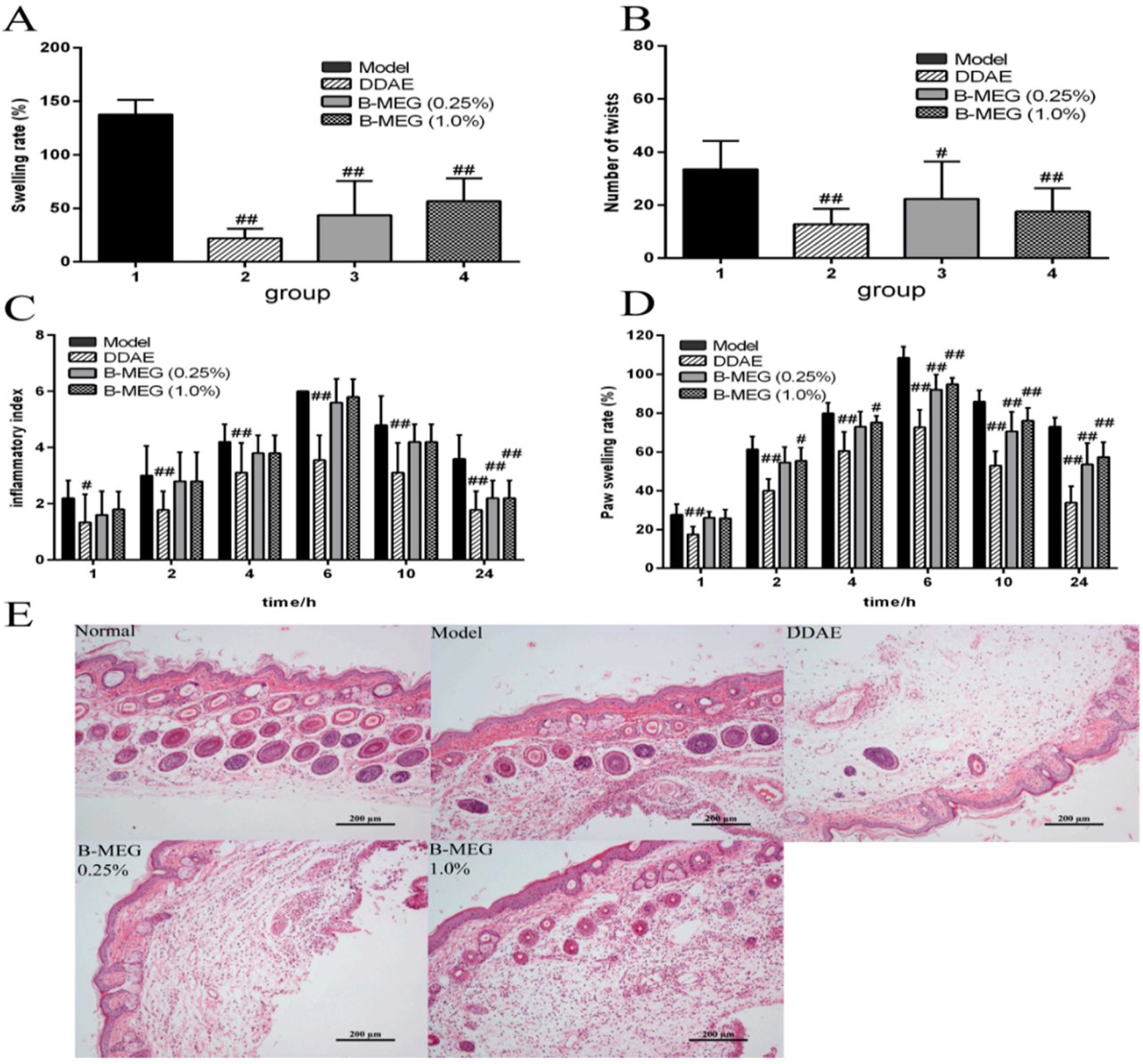

Fig. 7. *In vivo* efficacy of B-MEG in mice Note: (A) Effects of B-MEG on xylene-induced auricular swelling in mice ($x \pm s$, n = 10). (B) Effects of B-MEG on acetic acid induced writhing in mice ($x \pm s$, n = 10). (C) Effects of B-MEG on GA induced inflammation index of paw in mice ($x \pm s$, n = 10). (D) Effects of B-MEG on GA induced paw swelling rate in mice ($x \pm s$, n = 10). (E) GA induced histopathological examination of the paw mice in each group (H&E, 200 ×). DDAE is diclofenac diethylamine emulgel. Compared with the model group, $^{\#}P < 0.05$, $^{\#\#}P < 0.01$.

the mouse model of gout.

Hematoxylin and eosin staining revealed subcutaneous hyperplasia and extensive inflammatory cell infiltration in the gout model paw tissue (Fig. 7E). B-MEG treatment markedly reduced inflammatory cell infiltration when compared to model group, though less potently than DDAE. B-MEG suppressed inflammation in gouty arthritis which might occur through baicalin-mediated inhibition of NLRP3 inflammasome activation and IL-1β production (Wen et al., 2018).

4. Discussion

Unsuitable oil phase, surfactant and co-surfactant would lead to poor compatibility or low drug loading of microemulsion. Therefore, this study screened the solubility of baicalin in each phase, selected the microemulsion components, and investigated the compatibility of each component of the microemulsion, so as to ensure that the baicalin-loaded microemulsion (B-ME) maintained good stability under high drug loading concentration.

As a new method of experimental optimization, central composite design-response surface methodology (CCD-RSM) has been widely used in scientific research work. It is more simplified than orthogonal test and more comprehensive than uniform design (Fang et al., 2021). It has fewer test times and higher test accuracy, and is suitable for multi-factor and multi-level test (Mishra et al., 2023). Most importantly, it can also predict the results of unperformed tests (Liu et al., 2023). In this study, CCD-RSM was adopted, with oil phase and Km as factors, drug load and particle size as indicators, and design expert software was used to optimize the proportion of each phase of B-ME.

There are three methods to prepare microemulsion gel: (1) The gel matrix is added into the prepared microemulsion and fully swelled and stirred evenly (Daryab et al., 2022; Shinde et al., 2018); (2) The gel matrix is added into water and fully swelled, then mixed with the prepared microemulsion and stirred evenly (Cao et al., 2017); (3) the water phase of the microemulsion is first mixed with the gel matrix, then the

microemulsion gel is prepared according to the preparation method of the microemulsion (Niu et al., 2023). In this experiment, we compared these three preparation methods, and found that the second method would reduce the drug loading of microemulsion gel, and the microemulsion gel prepared by the third method was not uniform. Therefore, B-MEG was prepared by the first method, direct swelling method, which does not change the drug content, and the preparation was easier and more uniform.

In the early stage of this experiment, a variety of gel materials were screened, especially the commonly used Carbomer series gel matrix (Daryab et al., 2022). We found that B-ME had poor compatibility with the gel matrix of Carbomer series, which could not reach the ideal gel state and the solution tends to be turbid. This phenomenon had little relationship with the pH value of the solution as the blank microemulsion demonstrated good compatibility with the gel matrix of Carbomer. Baicalin may break the gel structure formed by Carbomer, and its mechanism needs to be further studied.

Split-plot design is an extension of block design and a comprehensive application of completely random block design and Latin square design. The split-zone design is characterized by simultaneous investigation of multiple factors and analysis of their interactions, effectively reducing the number of experiments (Goulão et al., 2018). In this experiment, tri-split-plot design method was used to screen the gel matrix and screen the type and dosage of transdermal agent. In view of the antibacterial and anti-inflammatory effects of borneol and clove oil, the two were selected as penetration enhancer in this study, in order to produce synergistic effect with baicalin in anti-gout pharmacological activity while promoting penetration in subsequent studies.

In this study, the skin penetration within 12 h of B-ME with penetration enhancer was about 1.52 times that of B-MEG with penetration enhancer, and 4.06 times that of B-MEG without penetration enhancer. With the combination of microemulsion technology and gel technology, compound permeator was used to effectively improve the drug carrying capacity and cumulative permeability of baicalin, B-MEG had obvious advantages when compared to the ordinary gel of baicalin prepared by Zhang et al (Zhang et al., 2015).

The topical efficacy of baicalin has been demonstrated through loading in various carriers for inhibition of skin inflammation, such as diethylene glycol monoethyl ether-mediated cubic phase gel (containing 2 mg/g baicalin) (Zhang et al., 2015), phospholipid vesicles (1 % baicalin) (Mir-Palomo et al., 2016), vaseline cream (2 % baicalin) (Hung et al., 2018), gellan-cholesterol nanohydrogel (1 % baicalin) (Manconi et al., 2018), and so on. To the best of our knowledge, the prescription and indication for B-MEG (1 % baicalin) have not been reported in the literature.

Nanomedicine offers unique opportunities for the treatment of noninfectious arthritis (Chen et al., 2021), including rheumatoid arthritis (RA) and GA. Transdermal delivery delivers therapeutics locally in a sustained manner, thus extending the half-life, improving bioavailability, and reducing the side effects of drugs for RA (Zhang et al., 2022) or GA (Liao et al., 2023).

In this paper, B-MEG groups at low and high dose significantly reduced the number of ear swelling induced by xylene and the number of body twisting induced by acetic acid in mice, and also significantly decreased the degree of toe swelling in mice GA model, but B-MEG did not show significant dose–effect relationship. The doses of B-MEG and DDAE were set by consulting references and doing pre-experiments. For example, in a mouse writhing experiment caused by acetic acid, curcuma microemulsion gel was administered at the doses of 0.12, 0.06 and 0.03 g/cm^2, respectively, on the abdominal skin of mice, and the administration area was 2 cm × 2 cm (Zhong et al., 2011). In a xylene-induced auricular swelling experiment in mice, the doses of DDAE and Flos Magnoliae oil-based microemulsion gel all were set to 0.2 g per mouse (Liang et al., 2019). According to the conversion of baicalin effective dose, the area of administration and the result of pre-experiment, different doses were set in different experiments, and the anti-inflammatory experimental dose was less than the analgesic experimental dose.

The anti-inflammatory and analgesic mechanism of B-MEG needs to be studied. Concentrations of the baicalin in the skin and joints or in the blood will be measured.

5. Conclusion

In this work, a baicalin-loaded microemulsion gel (B-MEG) was rationally designed using a combination of oils, surfactants, co-surfactants, gelling agents and permeation enhancers. The optimization of B-MEG resulted in enhanced baicalin solubility, skin permeation, and retention, thus improving its transdermal delivery. In anti-inflammatory and analgesic experiments, B-MEG had good efficacy and high safety. In acute gout model, B-MEG demonstrated significant anti-inflammatory effects by suppressing paw edema and inflammatory cell infiltration after topical application. B-MEG may improve baicalin bioavailability and effectiveness of baicalin through transdermal delivery, avoiding limitations of oral gout therapies. This optimized B-MEG system shows promise as a novel topical treatment for gouty arthritis.

CRediT authorship contribution statement

Yingzhou Wang: Writing – original draft, Methodology, Investigation, Formal analysis, Data curation, Conceptualization. **Mingxue Liu:** Writing – original draft, Methodology, Investigation, Formal analysis, Data curation, Conceptualization. **Junjie Li:** Writing – original draft, Software, Methodology, Investigation, Formal analysis, Conceptualization. **Peipei Jiang:** Software, Methodology, Investigation, Formal analysis, Conceptualization. **Di Han:** Software, Formal analysis. **Hongling Zhang:** Resources, Project administration. **Lingyun Xu:** Writing – review & editing, Validation, Supervision, Resources, Project administration, Methodology, Funding acquisition, Conceptualization. **Yinsheng Qiu:** Writing – review & editing, Supervision, Resources, Funding acquisition, Conceptualization.

Declaration of competing interest

The authors declare that they have no known competing financial interests or personal relationships that could have appeared to influence the work reported in this paper.

Acknowledgments

I would like to thank Pei Zhang and Bi-Chao Xu from the Core Facility and Technical Support, Wuhan Institute of Virology, for their help with producing TEM micrographs. We also thank Prof. Zhibing Zhang, Ms. Yi Tian Yap and Mr. Mohammad Abdulghani at the Department of Physiology, Wayne state university, USA, for their help with the manuscript revision.

Appendix A. Supplementary material

Supplementary data to this article can be found online at https://doi.org/10.1016/j.jsps.2024.102100.

References

Ali, Z., Din, F.U., Zahid, F., et al., 2022. Transdermal delivery of allopurinol-loaded nanostructured lipid carrier in the treatment of gout. BMC Pharmacol. Toxicol. 23 (1), 86–103. https://doi.org/10.1186/s40360-023-00680-z.

Ali, F.R., Shoaib, M.H., Yousuf, R.I., et al., 2017. Design, development, and optimization of dexibuprofen microemulsion based transdermal reservoir patches for controlled drug delivery. Biomed. Res. Int. 2017, 4654958. https://doi.org/10.1155/2017/4654958.

Bao, M.L., Ma, Y.F., Liang, M., et al., 2022. Research progress on pharmacological effects and new dosage forms of baicalin. Vet. Med. Sci. 8 (6), 2773–2784. https://doi.org/10.1002/vms3.960.

Cao, Y., 2021. Icariin alleviates MSU-induced rat GA models through NF-κB/NALP3 pathway. Cell Biochem. Funct. 39 (3), 357–366. https://doi.org/10.1002/cbf.3598.
Cao, M.Y., Ren, L.L., Chen, G.G., 2017. Formulation optimization and *ex vivo* and *in vivo* evaluation of celecoxib microemulsion-based gel for transdermal delivery. AAPS PharmSciTech. 18 (6), 1960–1971. https://doi.org/10.1208/s12249-016-0667-z.
Chen, L., Wang, Y.Z., Sun, L., et al., 2021. Nanomedicine strategies for anti-inflammatory treatment of noninfectious arthritis. Adv. Healthc. Mater. 10 (11), e2001732.
Daryab, M., Faizi, M., Mahboubi, A., et al., 2022. Preparation and characterization of lidocaine-Loaded, microemulsion-based topical gels. Iran J Pharm Res. 21 (1), e123787.
Fang, Z.Z., Huang, W.Z., Qi, J.P., et al., 2021. Progress on application of central composite design-response surface methodology in optimization of preparations in China. Acta Pharm. Sin. 56 (1), 169–177.
Fattori, V., Staurengo-Ferrari, L., Zaninelli, T.H., et al., 2020. IL-33 enhances macrophage release of IL-1β and promotes pain and inflammation in gouty arthritis. Inflamm. Res. 69 (12), 1271–1282. https://doi.org/10.1007/s00011-020-01399-x.
Ghias, M., Shah, S.W.A., Al-Joufi, F.A., et al., 2022. *In vivo* antistress effects of synthetic flavonoids in mice: behavioral and biochemical approach. Molecules. 27 (4), 1402. https://doi.org/10.3390/molecules27041402.
Goulão, B., MacLennan, G., Ramsay, C., 2018. The split-plot design was useful for evaluating complex, multilevel interventions, but there is need for improvement in its design and report. J. Clin. Epidemiol. 96, 120–125. https://doi.org/10.1016/j.jclinepi.2017.10.019.
Hmingthansanga, V., Singh, N., Banerjee, S., et al., 2022. Improved topical drug delivery: role of permeation enhancers and advanced approaches. Pharmaceutics. 14 (12), 2818. https://doi.org/10.3390/pharmaceutics14122818.
Hu, W., Bian, Q., Zhou, Y., et al., 2022. Pain management with transdermal drug administration: A review. Int. J. Pharm. 618, 121696 https://doi.org/10.1016/j.ijpharm.2022.121696.
Hung, C.H., Wang, C.N., Cheng, H.H., et al., 2018. Baicalin ameliorates imiquimod-induced psoriasis-like inflammation in mice. Planta. Med. 84 (15), 1110–1117. https://doi.org/10.1055/a-0622-8242.
Keinath, A.P., 2019. Integrated management of downy mildew on slicing cucumber with fungicides and host resistance but not trellising. Plant Dis. 103 (10), 2592–2598. https://doi.org/10.1094/PDIS-02-19-0323-RE.
Keller, S.F., Mandell, B.F., 2021. Management and cure of gouty arthritis. Med. Clin. North. Am. 105 (2), 297–310. https://doi.org/10.1016/j.mcna.2020.09.013.
Kováčik, A., Kopečná, M., Vávrová, K., 2020. Permeation enhancers in transdermal drug delivery: benefits and limitations. Expert. Opin. Drug Deliv. 17 (2), 145–155. https://doi.org/10.1080/17425247.2020.1713087.
Lan, X.X., Zhou, T.T., Dong, Y., et al., 2021. Dermal toxicity, dermal irritation, and delayed contact sensitization evaluation of oil body linked oleosin-hEGF microgel emulsion *via* transdermal drug delivery for wound healing. Cutan Ocul. Toxicol. 40 (1), 45–53. https://doi.org/10.1080/15569527.2021.1874008.
Li, X., He, Z., Ding, W.F., et al., 2020a. Assessment of dermal safety of oil extracted from *Periplaneta americana*: acute dermal toxicity, irritation, and sensitization. Cutan Ocul. Toxicol. 39 (3), 193–199. https://doi.org/10.1080/15569527.2020.1769126.
Li, Y.Y., Song, K., Zhang, H.L., et al., 2020b. Anti-inflammatory and immunomodulatory effects of baicalin in cerebrovascular and neurological disorders. Brain Res. Bull. 164, 314–324. https://doi.org/10.1016/j.brainresbull.2020.08.016.
Li, B., Wen, M., Li, W., et al., 2011. Preparation and characterization of baicalin-poly-vinylpyrrolidone coprecipitate. Int. J. Pharm. 408 (1–2), 91–96. https://doi.org/10.1016/j.ijpharm.
Liang, L.Y., Cai, H.X., Deng, J.R., et al., 2019. Development and pharmacodynamics of microemulsion gel of Xinyi oil. China J. New Drugs. 28 (23), 2899–2908.
Liao, S.J., Qiu, G.R., Hu, Y.P., et al., 2023. Separable and inseparable silk fibroin microneedles for the transdermal delivery of colchicine: development, characterization, and comparisons. AAPS PharmSciTech. 25 (1), 3. https://doi.org/10.1208/s12249-023-02716-3.
Lin, L., Asghar, S., Huang, L., et al., 2021. Preparation and evaluation of oral self-microemulsifying drug delivery system of Chlorophyll. Drug Dev. Ind. Pharm. 47 (6), 857–866. https://doi.org/10.1080/03639045.2021.1892746.
Liu,D.R., Liu, R.P., Zhuang, Z.B., et al., 2023. Preparation of self-microemulsion solids of kaempferia galanga (L.) volatile oil and its effect on rats with gastric ulcer. AAPS PharmSciTech. 29;24(8):243. DOI: 10.1208/s12249-023-02693-7.
Liu, Z.Y., Xiang, H.L., Deng, Q., et al., 2023b. Baicalin and baicalein attenuate hyperuricemic nephropathy via inhibiting PI3K/AKT/NF-κB signalling pathway. Nephrology. 28 (6), 315–327. https://doi.org/10.1111/nep.14159.
Lu, L.N., Zuo, Y.H., Wang, Y.X., et al., 2019. Simultaneous identification of the three active constituents in lung-ventilating-regulating oral liquid by RP-HPLC. Pak. J. Pharm. Sci. 32 (5), 2459–2464.
Manconi, M., Manca, M.L., Caddeo, C., et al., 2018. Nanodesign of new self-assembling core-shell gellan-transfersomes loading baicalin and in vivo evaluation of repair response in skin. Nanomedicine. 14 (2), 569–579. https://doi.org/10.1016/j.nano.2017.12.001.
Mi, X., Hu, M.G., Dong, M.R., et al., 2021. Folic acid decorated zeolitic imidazolate framework (ZIF-8) loaded with baicalin as a nano-drug delivery system for breast cancer therapy. Int. J. Nanomed. 16, 8337–8352. https://doi.org/10.2147/IJN.S340764.
Mir-Palomo, S., Nácher, A., Díez-Sales, O., et al., 2016. Inhibition of skin inflammation by baicalin ultradeformable vesicles. Int. J. Pharm. 511 (1), 23–29. https://doi.org/10.1016/j.ijpharm.2016.06.136.
Mishra, R., Prabhavalkar, K.S., Bhatt, L.K., 2016. Preparation, optimization, and evaluation of Zaltoprofen-loaded microemulsion and microemulsion-based gel for transdermal delivery. J Liposome Res. 26 (4), 297–306. https://doi.org/10.3109/08982104.
Mishra, R., Jain, N., Kaul, S., et al., 2023. Central composite design-basedoptimization, fabrication, and pharmacodynamic assessment of sulfasalazine-loaded lipoidal nanoparticle-based hydrogel for the management of rheumatoid arthritis. Drug Deliv. Transl. Res. 13 (4), 994–1011. https://doi.org/10.1007/s13346-022-01260-0.
Niu, J.X., Yuan, M., Gao, P.P., et al., 2023. Microemulsion-based keratin-chitosan gel for improvement of skin permeation/retention and activity of curcumin. Gels. 9 (7), 587. https://doi.org/10.3390/gels9070587.
Ou, S.P., Wang, S., Zhang, H.Y., et al., 2009. Determination and characterization of solubility of baicalin. Prog Mod Biomed. 20 (9), 3954–3957.
Ren, S., Meng, F., Liu, Y., et al., 2020. Effects of external application of compound Qingbi granules on acute gouty arthritis with dampness-heat syndrome: a randomized controlled trial. Chin Med. 15 (1), 117–130. https://doi.org/10.1186/s13020-020-00398-8.
Shinde, U.A., Modani, S.H., Singh, K.H., 2018. Design and development of repaglinide microemulsion gel for transdermal delivery. AAPS PharmSciTech. 19 (1), 315–325. https://doi.org/10.1208/s12249-017-0811-4.
Souto, E.B., Cano, A., Martins-Gomes, C., et al., 2022. Microemulsions and nanoemulsions in skin drug delivery. Bioengineering. 9 (4), 158–189. https://doi.org/10.3390/bioengineering9040158.
Špaglová, M., Čuchorová, M., Čierna, M., et al., 2021. Microemulsions as solubilizers and penetration enhancers for minoxidil release from gels. Gels. 7 (1), 26–43. https://doi.org/10.3390/gels7010026.
Szumała, P., Macierzanka, A., 2022. Topical delivery of pharmaceutical and cosmetic macromolecules using microemulsion systems. Int. J. Pharm. 615, 121488 https://doi.org/10.1016/j.ijpharm.2022.121488.
Talaat, S.M., Elnaggar, Y.S.R., Abdalla, O.Y., 2019. Lecithin microemulsion lipogels versus conventional gels for skin targeting of terconazole: *in vitro*, *ex vivo*, and *in vivo* investigation. AAPS PharmSciTech. 20 (4), 161–181. https://doi.org/10.1208/s12249-019-1374-3.
Tian, Z., Zhang, H.X., Shang, C., 2021. Farrerol ameliorate adjuvant-induced ankle injury via alteration of PPAR-γ signal pathway. J. Food Biochem. 45 (5), e13585.
Wan, T., Pan, J.T., Long, Y.M., et al., 2017. Dual roles of TPGS based microemulsion for tacrolimus: Enhancing the percutaneous delivery and anti-psoriatic efficacy. Int. J. Pharm. 528 (1–2), 511–523. https://doi.org/10.1016/j.ijpharm.2017.06.050.
Wang, J.Z., Li, Z.Y., Sun, F.F., et al., 2017. Evaluation of dermal irritation and skin sensitization due to vitacoxib. Toxicol. Rep. 4, 287–290. https://doi.org/10.1016/j.toxrep.2017.06.003.
Wang, Y.Z., Yu, R.F., Xiao, J.J., et al., 2022. Stability and rheological characteristics of baicalin loaded in microemulsion-based gel. Chin. J. Modern Appl. Pharmacy 39 (15), 1967–1973. https://doi.org/10.13748/j.cnki.issn1007-7693.2022.15.008.
Wei, Q., Zheng, Y.R., Ma, R.C., et al., 2021. Kinetics of proteolysis in stored Mongolian cheese at ice-temperatures and split-split-plot analysis of storage factors affecting cheese quality. Food Res. Int. 140, 109850 https://doi.org/10.1016/j.foodres.2020.109850.
Wen, X.P., Liu, D.J., Pei, Y.X., et al., 2018. Effect of baicalin on the expression of NLRP3 inflammsome and inflammatory factors in monosodium urate-induced raw264.7 macrophages. Chin. New Drug. 27(2):190-194.
Wen, X.P., Liu, D.J., Pei, Y.X., et al., 2017. Experimental study of baicalin on acute gouty arthritis. Chin. Med. Mat. 40 (8), 1952–1955.
Wen, Y.Q., Wang, Y.Z., Zhao, C.X., et al., 2023. The pharmacological efficacy of baicalin in inflammatory diseases. Int. J. Mol. Sci. 24 (11), 9317–9333. https://doi.org/10.3390/ijms24119317.
Wilson, L., Saseen, J.J., 2016. Gouty arthritis: A review of acute management and prevention. Pharmacotherapy. 36 (8), 906–922. https://doi.org/10.1002/phar.1788.
Xiang, H.L., Lei, H., Liu, Z.Y., et al., 2021. Network pharmacology and molecular docking analysis on molecular targets: Mechanisms of baicalin and baicalein against hyperuricemic nephropathy. Toxicol. Appl. Pharm. 424, 115594 https://doi.org/10.1016/j.taap.2021.115594.
Yang, J.H., Xu, H.H., Wu, S.S., et al., 2017. Preparation and evaluation of microemulsion–based transdermal delivery of cistanche tubulosa phenylethanoid glycosides. Mol. Med. Rep. 15 (3), 1109–1116. https://doi.org/10.3892/mmr.2017.6147.
Yang, H., Yi, H., Li, M.L., et al., 2007. Studies on effect of microemulsion in enhancing solubility of baicalin and puerarin. China J. Chin. Mater. Med. 32 (19), 1996–1999.
Zhang, Y.Y., Gao, Z.J., Chao, S.S., et al., 2022. Transdermal delivery of inflammatory factors regulated drugs for rheumatoid arthritis. Drug Deliv. 29 (1), 1934–1950. https://doi.org/10.1080/10717544.2022.2089295.
Zhang, Y.T., Zhang, K., Guo, T., et al., 2015. Transdermal baicalin delivery using diethylene glycol monoethyl ether-mediated cubic phase gel. Int. J. Pharm. 479 (1), 219–226. https://doi.org/10.1016/j.ijpharm.2014.12.055.
Zhong, H., Yin, R.L., Hou, Z.J., et al., 2011. Pharmacodynamic study of curcuma microemulsion gel. China Pharm. J. 20 (08), 26–27.